Biomaterials Science

ROYAL SOCIETY OF CHEMISTRY

PAPER

Cite this: *Biomater. Sci.*, 2025, **13**, 6458

Impact of material characteristics on nanoparticle penetration and retention in thrombi: implications for thrombolysis

Xiangxun Chen, [a,b] Haotian Cha, [b] Shehzahdi S. Moonshi, [a,b] Nam-Trung Nguyen [b] and Hang Thu Ta *† [a,b]

Received 7th August 2025,
Accepted 29th September 2025

DOI: 10.1039/d5bm01192b

rsc.li/biomaterials-science

Ischemic cardiovascular disease is the leading cause of death worldwide and is primarily attributed to blood vessel occlusion caused by thrombi. While current treatments and research focus on overall thrombolytic activity, they often overlook the distribution of therapeutic agents or drug-loaded nanomaterials within the thrombus. This study is the first to systematically investigate how the material, size, shape, and charge of nanoparticles affect their ability to penetrate and distribute within a thrombus. The ultimate goal is to guide the development of more efficient thrombolytic nanomaterials. Recently, various metal (*e.g.* gold and silver) and metal oxide nanomaterials have been developed for thrombolysis and molecular imaging of thrombi. Based on this, we employed gold and silver nanoparticles in our study. Nanoparticles ranging from 10 to 200 nm in size, with both positive and negative surface charges, and in spherical and rod-shaped forms, were evaluated using two-photon microscopy, loop-based diffusion, and both static and dynamic microchannel thrombus models. It was found that the physicochemical characteristics of nanoparticles strongly influence their ability to penetrate and accumulate within the thrombus. In particular, the larger the particle size, the lower the penetration and the higher the retention. Negative surface charge and silver materials favour penetration of the particles compared to positively charged or gold particles, respectively. Particle shape is also an influence factor, where a rod shape reduces penetration and increases retention. These findings provide valuable insights for designing future diagnostic and therapeutic nanoparticles.

1. Introduction

A thrombus occluding blood flow is the underlying physiological explanation for cardiovascular diseases such as ischemic stroke, venous thrombosis, and myocardial infarction, which are the leading causes of death worldwide.[1] Current thrombolytic options include the use of tissue plasminogen activator (tPA), which remains the only FDA-approved therapeutic agent for ischemic stroke.[2] However, this gold standard still has some drawbacks. tPA is rapidly cleared from the human body due to its short half-life, necessitating frequent administration to maintain its therapeutic efficacy.[3] Moreover, the precise timing of drug delivery is crucial. For example, tPA must be administered within 4.5 hours of symptom onset and is only effective in approximately one-third of patients.[4] Alternative options to preserve its activity are needed for life-threatening situations. Therefore, nanoparticles (NPs) have received attention as an emerging option for drug delivery due to their permeability and ability to load different types of cargo.[5] Additionally, various metal (*e.g.* gold and silver) and metal oxide nanomaterials have been developed for thrombolysis and molecular imaging of thrombi.[6–17]

Most of the research to date has mainly focused on targeting thrombus components to achieve thrombolysis.[6,9,18,19] The main components of a thrombus are aggregated platelets and red blood cells and a mesh of cross-linked fibrins.[20] To efficiently deliver drug cargos to the clot, it is essential that the carrier or nanomaterial can both adhere to and penetrate deeply into the thrombus. However, the distribution of nanoparticles within a thrombus—particularly their precise location and concentration—remains poorly understood. Previous studies have attempted to image targeted particles on thrombi but have been unable to accurately pinpoint their exact location.[7,8] In addition, it is not known how the physico-

[a]*School of Environment and Science, Griffith University, Nathan Campus, Brisbane, Queensland, QLD 4111, Australia. E-mail: h.ta@griffith.edu.au; Tel: +61 (7) 3735 5384. https://hangta.group/, https://experts.griffith.edu.au/27034-hang-ta*

[b]*Queensland Quantum and Advanced Technologies Research Institute, Griffith University, Brisbane, Queensland, QLD 4111, Australia*

†Australian Research Council (ARC) Future Fellow and Australian Heart Foundation Future Leader Fellow.

chemical characteristics such as material, size, shape and charge of a nanomaterial affect its penetration and retention in a clot.

In this study, we aim to fill this knowledge gap by investigating the material, size, charge and shape-dependent NP dynamics in thrombi. This understanding can provide insight and guidance for designing effective drug delivery systems for thrombolysis applications. Here, we employ gold and silver NPs in the size range of 10–200 nm with varying electrical surface charges (positive and negative) and shapes (sphere and rod) to examine the abilities of the NPs to penetrate thrombi using different *in vitro* models.

2. Materials and methods

2.1. Chemicals

Gold (10 nm PEG-coated, 30 nm PEG-coated, 30 nm branched polyethylenimine-coated, and 100 nm PEG-coated) and silver (100 nm and 200 nm PEG-coated) NPs were purchased from nanoComposix (San Diego, CA, USA). Sodium borohydride ($NaBH_4$, 452874) was obtained from Aldrich. Hexadecyltrimethylammonium bromide (CTAB, H6269) and L-ascorbic acid (255564) were purchased from Sigma. Actin was acquired from Siemens (B4219-1).

2.2. Synthesis of gold nanorods

Gold nanorods were synthesised according to Mackey *et al.*[21] A seed solution containing 750 mL of 0.2 M CTAB, 250 mL of 1.0 mM $HauCl_4$ and 60 mL of 0.01 M $NABH_4$ was prepared. 16 mL of the seed solution was added to a growth solution (1000 mL of 1.0 mM $HauCl_4$, 1000 mL of 0.2 M CTAB, 45 mL of 4.0 mM silver nitrate, and 28 mL of 78.8 mM ascorbic acid), which was incubated overnight at room temperature. The obtained gold nanorods were verified by an absorbance reading (with a longitudinal peak of 780 nm) and washed by centrifugation at 15 000*g* for 15 minutes with water. The washed rods were redispersed in the same volume of liquid before washing, followed by the addition of thiol-PEG-COOH solution (gold nanorod : PEG-COOH, 1 : 1 mass ratio), which was incubated overnight to acquire PEGylated gold nanorods with a zeta potential of −3.4 ± 1.0 mV.

2.3. *In vitro* thrombus formation

The protocol was modified from the existing literature.[9,22] Human blood was obtained from the Australian Red Cross and approved by the Griffith Ethics Committee (2021/598) for research purposes. The whole blood was centrifuged for 15 min at 250*g* to obtain platelet-rich plasma. A thrombus mixture including 70 μL of the human plasma, 1 μL of 1 M calcium chloride ($CaCl_2$), and 3 μL of the actin was incubated at 37 °C for 1 h. The thrombus was then washed with PBS solution at room temperature with rotation for half an hour. The washed thrombus was then utilised for different assays.

2.4. Two-photon microscopy for permeation and analysis

The thrombus prepared using the methods stated in section 2.3 was transferred into a 96-well plate. The thrombus was incubated with 70 μL of the NP solution (concentrations are specified in the results) overnight. The thrombus was moved to another well for washing with 70 μL of PBS three times with gentle movement by hand. Finally, it was fixed with a 2% PFA solution and then transferred to a Zeiss LSM 710 Microscope with a Mai Tai (Spectra Physics, Newport) eHP DeepSee laser and a dedicated detector. Sub-100 fs pulses of 820 nm light were used for excitation, while the 2-photon luminescence of AuNPs was collected between 450 and 600 nm. Moreover, the silver NPs were excited using 780 nm laser light and their luminescence was collected between 420 and 780 nm.

The *Z*-stack images of each thrombus were obtained using a 10× objective. Each stack image had a 5 μm interval, and a total distance of 250 μm was imaged. FIJI was used to analyse the integrated intensities of the acquired images and normalised them for quantitative analysis. For more region-specific analysis, one ROI close to the edge of the thrombus and a ROI that represented the inside of the thrombus were selected based on the acquired image. The normalised values were calculated based on the intensity acquired in the ROI divided by the intensity of the standard NP sample at the same concentration in the 96-well plate.

2.5. Retention and analysis

NP retention refers to the ability of NPs to be trapped or held within a blood thrombus.[23] The thrombus obtained from section 2.3 was transferred to the following setup. A V-shaped polydimethylsiloxane (PDMS) channel was formed with the aid of a pre-treated 200 μL tip (QSP). The PDMS channel was fabricated using standard soft-lithography techniques.[24,25] Briefly, the PDMS mixture was made with a base part (SYLGARD 184 Silicone Elastomer base, 1317318) and a curing agent (SYLGARD 184 Silicone Elastomer curing agent, 1317318) at a weight ratio of 10 : 1, followed by 20 min vacuum degassing. Subsequently, the processed PDMS mixture was poured over the tip mould, where the 200 μL tip was positioned in a 55 mm Petri dish (PS, gamma sterile) (Fig. 1). The tip was pre-sprayed with WD-40 lubricant to make the surface more hydrophobic and facilitate easy stripping. The PDMS mixture was poured over the tips and baked in an oven at 70 °C for over 2 hours. After curing, the tips were taken from the PDMS model using needle nose pliers. The PDMS channel was arranged at the tube clamp stand, where the clamps hold the PDMS model vertically.

The formed channel was washed by filling it with water and incubated with collagen (300 μg mL^{-1}) solution for 10 min. Then, it was washed with PBS for better adhesion of the thrombus in the channel. The preformed thrombus was transferred to the middle of the channel straight after the washing process. The concentration of the flowthrough NPs was measured using a plate reader to obtain the retention of the NPs. The sample reading was divided by that of a standard

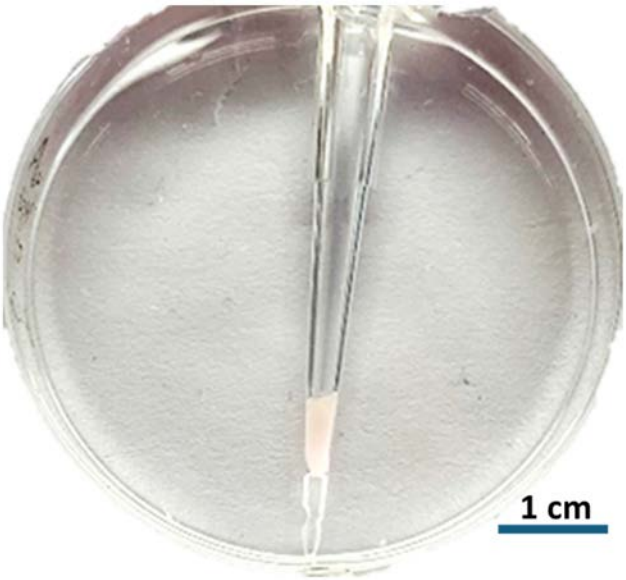

Fig. 1 Representative image of the tip channel with a thrombus within the channel.

sample (pure NP solution) at the same concentration and wavelength to obtain the normalised value of the sample itself compared to its standard.

2.6. Static diffusion and analysis

Fibrin thrombi were formed around steel inoculation loops from samples of human plasma (70 μL), 1 μL of 1 M $CaCl_2$ and 3 μL of actin in the presence of AuNPs (0.25 mg mL^{-1}), according to the procedure modified from ref. 26. The fibrin thrombus was formed after the mixture of the above solution and the loop was incubated at 37 °C for 1 h. The thrombus was dialysed for 24 h with PBS solution and the PBS was changed at 12 h. The thrombus was digested with trypsin at 37 °C. The NP content was quantified by dividing the absorbance reading of the sample by that of the standard sample (peaks provided by the companies, Table 1) at the same concentration and wavelength.

2.7. Diffusion under flow and analysis

A straight microfluidic channel model was used to mimic the internal environment of blood vessels. The dimensions of the channel were 30 mm × 1.5 mm × 3.5 mm (length × width × height). The channel model was fabricated by laser cutting (CO_2 laser cutting machine, Rayjet 300, Trotec) on PMMA laminates. Next, the PMMA strips were adhered onto a petri dish with super glue (Loctite precision super glue) and treated with WD-40 lubricant for easily removing the PDMS channel from its surface. Subsequently, the PDMS mixture was poured over the model, and the procedure was the same as the tip channel in section 2.5. After peeling off the PDMS from the mould, inlet and outlet holes were punched. Next, the channel was treated with 100 μL of collagen (300 μg mL^{-1}) for 10 min to make it more hydrophilic for the thrombus to adhere followed by three PBS washes. The PDMS layer and glass substrates were treated for 45 seconds with 18 W plasma using a plasma cleaner (Harrick Plasma). The freshly developed thrombus described in section 2.3 was transferred to the treated channel before the final integration of the channel with the glass substrate. Finally, tubing was attached to the inlet and outlet of the channel and was further connected with a peristaltic pump for continuous flow. A peristaltic pump (NE-9000) was used to pump through a channel with various nanoparticle solutions with the same concentration of 0.25 mg mL^{-1} in PBS for 4 h at a flow rate of 31 μL min^{-1}, corresponding to a physiological arterial base wall shear rate of 1000 s^{-1}. A control group with PBS was infused into the channel for 4 h.

2.8. Statistical analysis

Data are presented as mean ± standard error of the mean. One-way ANOVA with *post hoc* Dunnett's or Tukey's and a *T* test were employed. The statistical test for each parameter is stated in each figure legend for significance testing, with a p value of ≤ 0.05 considered statistically significant. Data analyses were performed using GraphPad Prism (GraphPad Software Inc.).

3. Results and discussion

To study the effect of the size, shape, charge and material of NPs on their capability to penetrate and remain in the thrombus, we employed 7 different NPs as described in Table 1.

In this study, we employed an *in vitro* human thrombus model representing an arterial thrombus, or a "white" thrombus, which is primarily composed of platelets and fibrin. For this reason, red blood cells were not included. Our focus on arterial thrombi is based on the fact that they are responsible for life-threatening cardiovascular events such as heart attack, myocardial infarction and ischemic stroke.

3.1. Spatial distribution of NPs within thrombi visualised by two-photon microscopy

Previously, two-photon microscopy was utilised to visualise deep tissues in animal models with greater precision and less invasiveness than conventional confocal microscopy. This technique demonstrated the ability to locate different types of metallic NPs.[27,28] Additionally, studies have explored the use of two-photon microscopy to investigate thrombus formation and the associated microenvironmental changes.[29–31]

Here, to assess the three-dimensional distribution of NPs within the thrombus, two-photon microscopy was employed. The normalised intensity was calculated based on the standard NP intensity at the same concentrations. A distance of 250 μm across a thrombus from the bottom to the top was imaged with 5 μm intervals. The intensity of the whole imaged area was normalised to the standard (Fig. 2). By analysing the normalised intensities of NPs at different depths within the thrombus, we assessed how NP size and concentration affect their penetration.

3.1.1. Impact of particle sizes, materials, and charges on the overall distribution. To investigate the effect of NP size, we

Table 1 Characteristics of NPs employed in the study

Nanoparticles	Material	Size, nm	Charge, mV	Wavelength, nm	Shape
AUGN10	Gold	11.0 ± 0.7	−16	518	Sphere
AUGN30		32.7 ± 3.6	+25.1	522	
AUBB30		30 ± 3	65	520	
AUGN100		100 ± 11	−31	565	
AUNR		Length: 23 ± 5 Width: 8 ± 2	−3.4 ± 1.0	762	Rod
AGGN100	Silver	99 ± 10	−17	485	Sphere
AGGN200		197 ± 25	−19	485	

AUGN: negatively charged gold nanospheres with a PEG coating, AUBB: positively charged gold nanospheres with a BPEI coating, AGGN: negatively charged silver nanospheres with a PEG coating, and AUNR: negatively charged gold nanorods.

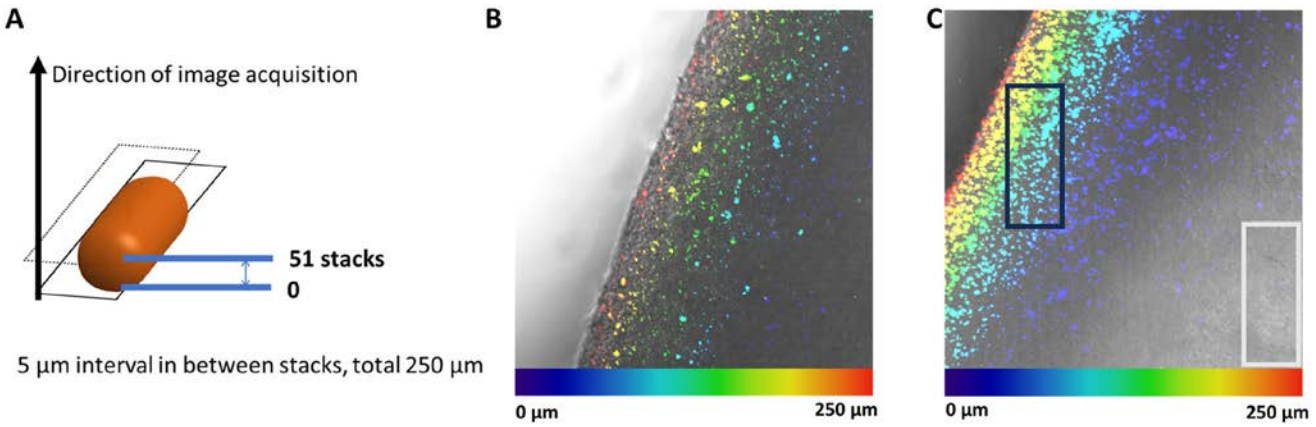

Fig. 2 Two-photon microscopy visualisation. (A) Schematic representation of the image acquisition direction. (B and C) Representative images of thrombi incubated with 30 nm branched polyethylenimine-coated gold NPs at concentrations of (B) 0.05 mg mL^{-1} and (C) 0.25 mg mL^{-1}, displayed in temperature colour mode. The representative ROIs of the inside (gray) and edge (black) were as indicated in bold rectangles (65.4 μm × 166.3 μm), with the same distance between the centre of the two ROIs (330 μm).

examined the distribution profiles of AuNPs with negative charge and different sizes (10, 30 and 100 nm, Fig. 3A, B and G–I). The overall intensity of the NPs at various depths of the thrombus was first analysed. At both low (0.05 mg mL^{-1}) and high (0.25 mg mL^{-1}) NP concentrations, most NPs exhibited a generally decreasing trend in intensity with increasing depth (*Z*-axis) within the thrombus.

At low concentrations, smaller NPs generally exhibited better penetration. AUGN10 NPs showed the highest penetration (the intensity values ranged from 0.4 to 1.0, Fig. 3A) among the gold NPs, while AGGN200 showed the lowest. Both AUGN100 and AGGN100 groups displayed decreasing penetration trends with increasing depth. Compared to AUGN100, AGGN100 penetrated deeper into the thrombus as evidenced by the higher normalised intensity across the thrombus. At a high concentration (0.25 mg mL^{-1}), a similar trend was observed.

Positively charged NPs exhibited less penetration than negatively charged NPs. For both NPs, at low concentration, the NP distribution was even from the edge to the middle of the clot. When increasing the concentration to 0.25 mg mL^{-1}, NP penetration reduced as it reached further inside the clot. A high concentration of NPs showed a more obvious effect on their penetration.

Overall, these findings highlight the complex interplay between nanoparticle size, material, and charge in determining their penetration and distribution within the *in vitro* thrombus.

3.1.2. Impact of the sizes of particles on their penetration at the edge and inside ROIs. To further investigate the intra-thrombus distribution, we analysed the normalised intensity within specific regions of interest (ROIs): the thrombus centre (inside) and periphery (edge). Overall, the intensity of NPs within the thrombus decreases with increasing depth, with some variations at low and high concentrations.

Fig. 4 shows the intensity difference with increasing thrombus depth. At the low concentration (0.05 mg mL^{-1}) of AUGN10, the intensity at the thrombus edge exhibited a steady decrease from a normalised value of 0.32 at the bottom (0 μm) to 0.19 at the top (250 μm, Fig. 4A). Similarly, the intensity within the thrombus core also decreased (from 0.31 at the bottom to 0.11 at 250 μm). The trend for the high concentration (0.25 mg mL^{-1}) of AUGN10 was similar.

As the nanoparticle size increased to 30 nm and 100 nm, the intensity at the edge at low concentrations was lower than that of the 10 nm group (Fig. 4B and G), indicating reduced penetration of larger particles. This trend was also

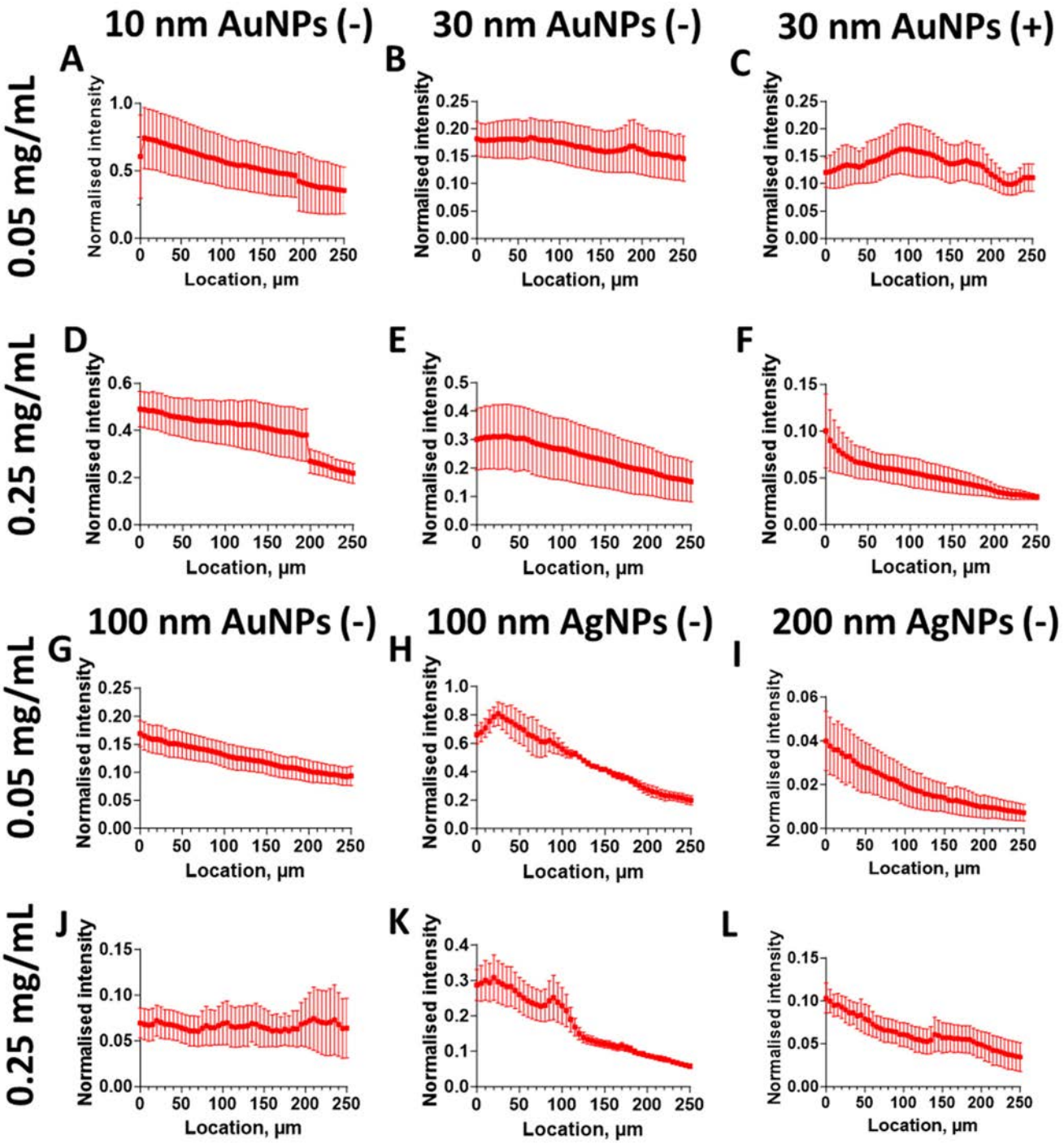

Fig. 3 Overall normalised intensity profiles of gold (AuNPs) and silver (AgNPs) NPs within the clots. NPs with varying concentrations (A–C and G–I) 0.05 mg mL^{-1} and (D–F and J–L) 0.25 mg mL^{-1}, different sizes and charges were evaluated. Two-photon microscopy was employed to measure the nanoparticle distribution along the *z*-axis of the clot, with data points collected at 5 μm intervals up to a depth of 250 μm. The normalised intensity represents the relative nanoparticle concentration at each location. Error bars indicate standard deviation (n = 3–4 per group).

observed for increased nanoparticle concentrations (Fig. 4D, E and J).

For silver NPs, as the size increased from 100 nm to 200 nm, the 200 nm group exhibited a similar decreasing trend at both the edge and inside, with lower intensity compared to the 100 nm silver group. Both 100 nm gold and silver NPs showed a decreasing trend within the thrombus core, while the gold NP group exhibited a lower intensity than the silver group at both the edge and inside area (Fig. 4G and H). But the high concentration of AUGN100 had a more stable trend throughout the imaged thickness (Fig. 4J and K).

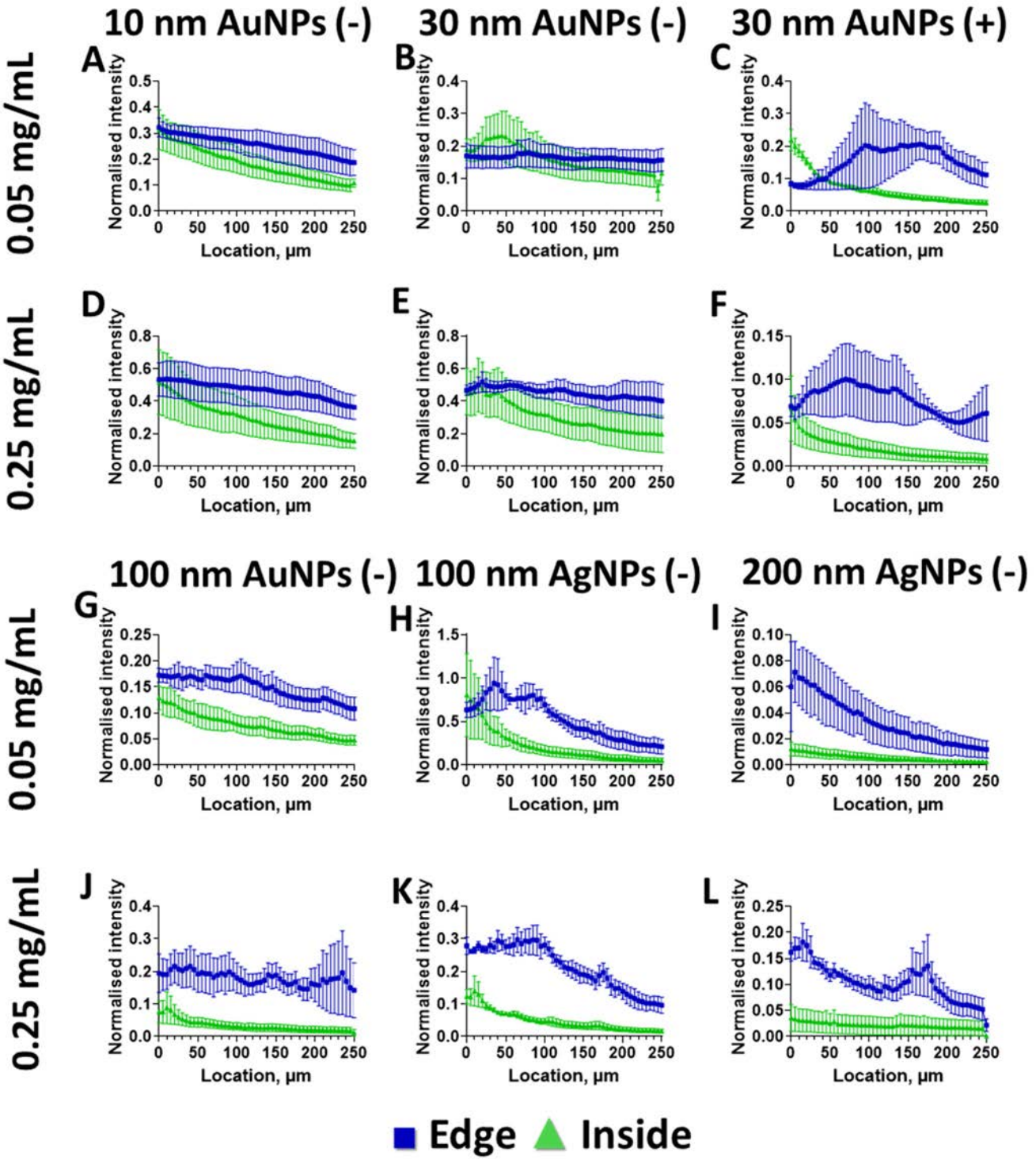

Fig. 4 Normalised intensity profiles of gold NPs (AuNPs) and silver NPs (AgNPs) within the thrombus with the edge and inside ROI. NPs with varying concentrations ((A–C and G–I) 0.05 mg mL^{-1} and (D–F and J–L) 0.25 mg mL^{-1}), sizes and surface charges were evaluated: negatively charged (–) (A and D) 10 nm, (B and E) 30 nm, (C and F) positively charged (+), (G and J) 100 nm AuNPs; (H and K) 100 nm AgNPs, and (I and L) 200 nm AgNPs. Two-photon microscopy was employed to measure the nanoparticle distribution along the *z*-axis of the clot, with data points collected at 5 μm intervals up to a depth of 250 μm. The normalised intensity represents the relative nanoparticle concentration at each location. Error bars indicate standard deviation (n = 3–4 per group).

Overall, these results highlight the influence of the size of particles on their penetration and distribution within thrombi. Smaller NPs, such as AUGN10, exhibited better penetration.

3.1.3. Impact of the zeta potential of particles on their penetration at the edge and inside ROIs. To investigate the influence of NP surface charge, we compared the penetration profiles of AUGN30 with those of AUBB30 (described earlier). At a low concentration (0.05 mg mL^{-1}), the negatively charged NPs (AUGN300) (Fig. 4B) exhibited minimal variation in normalised intensity at the thrombus edge. The intensity remained relatively constant, ranging from 0.17 at the bottom (0 μm) to 0.16 at the top (250 μm). The behaviour at the high concentration (0.25 mg mL^{-1}) differed slightly (Fig. 4E). Here, the normalised intensity at the periphery showed a slight initial decrease, followed by a modest increase.

The normalised intensity of positively charged NPs (AUBB30) (Fig. 4C and F) increased from the bottom to 95 μm (0.08 to 0.27), then remained at a similar level of around 0.25 until 190 μm, and then started to decrease until 250 μm. The high concentration of AUBB30 remained stable at 0.08 from the bottom to 10 μm, followed by an intensity rise to 0.09 at 140 μm. Then, the intensity started to decrease to 0.06 at 250 μm. Positively charged NPs displayed a markedly different behaviour. This trend persisted throughout the thrombus thickness, even at high concentration.

In summary, these results highlight the critical role of zeta potential or surface charge in nanoparticle penetration and distribution within thrombi. Negatively charged NPs exhibit enhanced penetration and accumulation compared to positively charged particles.

3.1.4. Impact of the material of particles on their penetration at the edge and inside ROIs. To investigate the influence of NP material on thrombus penetration, we compared negatively charged 100 nm gold and silver NPs (AUGN100 and AGGN100, respectively).

Our findings reveal distinct patterns based on nanoparticle type. Fig. 4G shows that the low concentration of AUGN100 exhibited an overall decreasing trend for both the edge and interior. On the other hand, for the edge, from the bottom to the top of the thrombus, AGGN100 showed an initial increase in intensity, followed by a subsequent decrease (Fig. 4H). At high NP concentration, the trend was similar (Fig. 4J and K). Additionally, the intensity range at the edge of the low-concentration AGGN100 group was higher than that of the AUGN100 group, suggesting greater penetration of nanoparticles into the edge region. The subsequent reduction in edge intensity and the low interior intensity of the AGGN100 group may be attributed to the abundance of silver nanoparticles penetrating the superficial edge region, potentially causing a blockage in the fibrin network and hindering further nanoparticle retention within the thrombus. Future studies can investigate this hypothesis. Overall, these results highlight the influence of nanoparticle type on their penetration and distribution within thrombi.

To the best of our knowledge, this is the first proof-of-concept study utilising two-photon optical imaging to visualise gold and silver NPs within *in vitro* thrombi. Generally, nanoparticle penetration into the thrombus decreases with depth, as indicated by the reduced normalized intensity of the inner regions of interest (ROIs) for each nanoparticle with increasing height. Smaller NPs and negatively-charged ones penetrate better than the larger and the positively-charged ones, respectively. Silver NPs exhibit better penetration than gold NPs at the same size and charge.

The current study utilised the same components for thrombus formation throughout the work as described in section 2.3. The thrombus was a grain-shaped mesh-like protein structure, where the network acted as a barrier to prevent the deeper penetration of the NPs into the clot. The outer regions of the thrombus may be looser compared to the interior, resulting in a higher NP intensity compared to the interior of the thrombus. The main components of human plasma include plasma proteins, platelets, fibrinogen/fibrin, factor VIII and factor V,[20] which were all rich in negative charges.[32,33] This explains why the positively-charged NPs (AUBB30) showed less penetration than the negatively-charged ones (AUGN30). We hypothesise that the positively-charged NPs may quickly encounter weak electrostatic interactions with the negatively charged component of the thrombus, blocking the thrombus pores and preventing further NP penetration.

Further studies may assess the nanoparticle interaction using different thrombus component models, such as those with red blood cells.

3.2. Permeability and retention of NPs in a thrombus tip model

The penetration capability of NPs into the thrombus was further assessed using a tip model (Fig. 5A) to measure the amount of NPs that stayed in the thrombus, which helps assess the impact of size, charge and types of NPs on thrombus retention within 4 h (Fig. 5B). In this model, the penetration of NPs into the thrombus was facilitated by gravity.

3.2.1. Impact of particle size. As the NP size increased, a greater proportion of the particles remained trapped in the thrombus and were unable to pass through.

At a concentration of 0.05 mg mL^{-1}, the AUGN10 retention was only 3.6% within the clot, while the AUGN30 retention was 27.5% ± 5.0 and the AUGN100 retention was 30.9% ± 4.4%. However, the same was not observed for silver NPs. In particular, AGGN100 did not show a significant increase in retention compared to AGGN200 (26.0% ± 1.9% *vs.* 23.5% ± 2.6%, respectively, Fig. 5B).

When the concentration was increased to 0.25 mg mL^{-1}, 51.3% of AUGN10 stayed in the thrombus. The AUGN30 retention (41.9% ± 0.2%) was not higher than the AUGN10 retention. The AUGN100 was retained significantly more than AUGN10 and AUGN30. Similarly, it was observed that AGGN200 exhibited greater retention or less passage through the thrombus compared to AGGN100 (Fig. 5B). These findings suggest that the retention effect is positively correlated with the increase of the nanoparticle size.

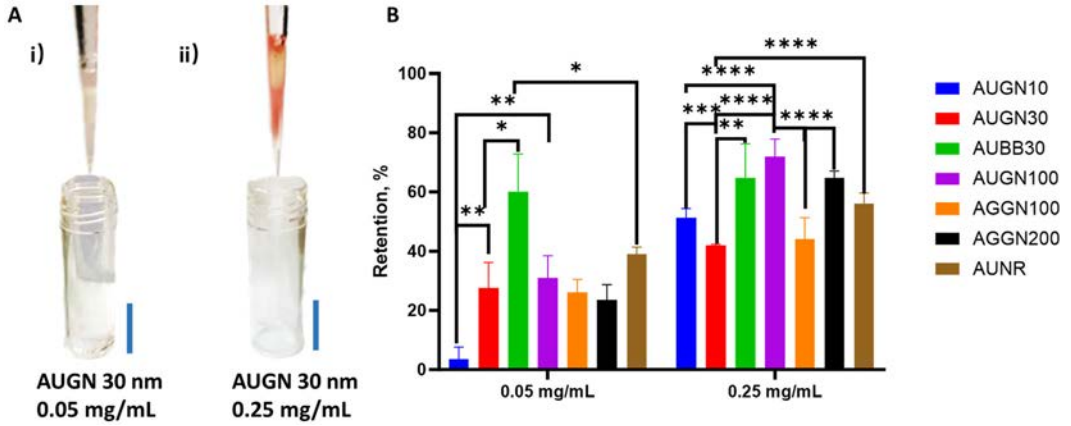

Fig. 5 Nanoparticle permeability in a thrombus tip model. (A) Representative image of the model with AUGN30 at concentrations of (i) 0.05 mg mL^{-1} and (ii) 0.25 mg mL^{-1} (blue scale bar: 1 cm). (B) % of NPs retained in the thrombus after complete flow through under gravity. AUGN: negatively charged gold nanospheres with a PEG coating; AUBB: positively charged gold nanospheres with a BPEI coating; AGGN: negatively charged silver nanospheres with a PEG coating; and AUNR: negatively charged gold nanorods. *, **, ***, and ****: $p < 0.05$, 0.01, 0.001 and 0.0001, respectively.

3.2.2. Impact of particle zeta potential. AUBB30 exhibited a significantly higher percentage of NP retention compared to AUGN30 at both low and high concentrations (Fig. 5B), exceeding 60%, with no significant difference observed between these concentrations. The data demonstrate that positively charged NPs have an enhanced retention effect in the thrombus. This is probably due to their increased affinity (electrostatic interaction) with the negatively-charged components of the thrombus.

3.2.3. Impact of particle material and shape. Fig. 5B shows that gold NPs (AUGN100) generally exhibited lower permeability compared to silver NPs (AGGN100). This material effect was stronger at high concentration than at low concentration; particularly, it was observed that AGGN100 was retained less or passed through the thrombus significantly more than AUGN100 (Fig. 5B).

Additionally, we found that NP shape influences its permeability and retention in the thrombus as well. Our synthesised gold nanorods (AUNR: 23 nm length and 8 nm width) showed reduced permeability relative to spherical NPs (AUGN10 and AUGN30) at both high and low concentrations.

The results presented in this section provide valuable insights into the factors influencing nanoparticle permeability within a static thrombus. Future studies can fully delve into the thrombus microstructure and nanoparticle–thrombus interactions. A deeper understanding of these mechanisms will be instrumental in refining nanoparticle design for optimal thrombus targeting and therapeutic outcomes.

3.3. Nanoparticle retention and diffusion in a loop model

This study evaluated the retention ability of various NPs in the thrombus and their ability to diffuse out into physiological solutions at different time points. Retention and diffusion are closely interconnected processes.[34,35] The extent to which NPs are retained within a thrombus will directly influence their ability to diffuse and the movement of NPs within a blood clot. In this model, NPs were incubated with the thrombosis materials to form a thrombus before undergoing dialysis (Fig. 6).

Similar to the previous 2 models, in this loop model, the effects of particle size, surface charge, material and shape were also observed, consistent with the findings from the other 2 models. In particular, after 12 h, the retention of gold and silver NPs showed a size-dependent effect, whereby an increase in the size of the NPs resulted in more NP retention in the blood clot. Later at 24 h, most of them slightly diffused out but the size-dependent retention trend remained.

The NP surface charge or zeta potential significantly impacted the NP retention. After 12 h, the positively charged gold NPs (AUBB30) showed 99.0% ± 0.2% retention, while the negatively charged ones (AUGN30) showed much lower retention (60.9 ± 4.9%). After 24 h, only 15.0% ± 2.1% of AUBB30 diffused out, marking the lowest diffusion rate over time. Interestingly, taken together, AUBB30 showed the highest retention amongst all NPs and even higher than the much larger NPs (AUGN100, AGGN100 and AGGN200).

Again, findings from this model show that NP material affected their retention. AUGN100 exhibited 27.5% diffusion after 24 h, an improvement from their 12 h results. However, when compared to AGGN100, the gold nanospheres were retained significantly more in the thrombus at both 12 (58.9% ± 12.5% *vs.* 72.5% ± 5.1%, respectively) and 24 h (21.6% ± 1.0% *vs.* 45.0% ± 1.2%, respectively). Interestingly, compared to all other NPs, AGGNP100 had the highest diffusion rate and lowest retention in the clot. Increasing the silver nanoparticle size from 100 nm to 200 nm led to a higher retention rate in the thrombus (21.6% ± 1.0% *vs.* 77.9% ± 1.3%, respectively).

Consistent with the finding from the previous model, NPs with a rod shape were retained more in the thrombus compared to spherical ones. The AUNRs showed a higher percentage of retention effect than AUGN30 at 12 h (72.7% ± 10.9% *vs.* 60.9 ± 4.9%, respectively). At 24 h, although a significant

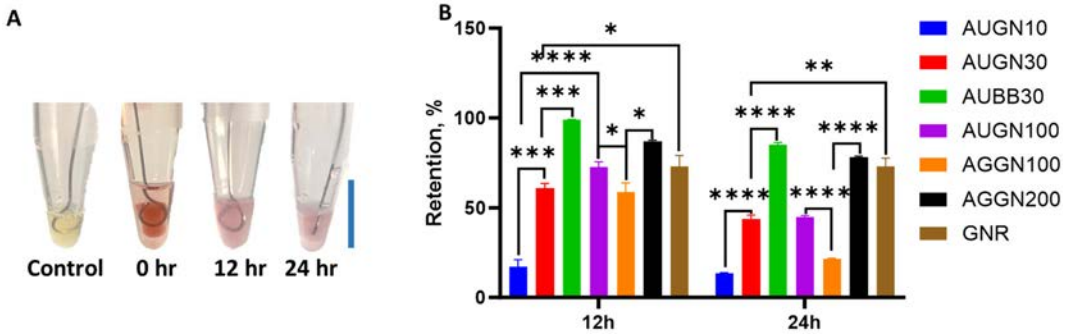

Fig. 6 Nanoparticle diffusion and retention in a human plasma thrombus. (A) Representative images of the loop-diffusion model from left to right: PBS control, AUGN30 (0.25 mg mL^{-1}) at times 0, 12 hours and 24 hours in PBS solution (blue scale bar: 1 cm). (B) Percentage of particle retention in the synthesised thrombus at 12 and 24 hours (n = 3 per group). AUGN: negatively charged gold nanospheres with a PEG coating, AUBB: positively charged gold nanospheres with a BPEI coating, AGGN: negatively charged silver nanospheres with a PEG coating, and AUNR: negatively charged gold nanorods. *, **, ***, and ****: p < 0.05, 0.01, 0.001 and 0.0001, respectively.

amount of AUGN30 diffused out of the thrombus, AUNRs did not and 72.7% ± 8.3% of their particles were retained.

Overall, AUBB30 demonstrated the highest retention, comparable to AGGN200. This suggests that particle size and surface charge play crucial roles in influencing their penetration behaviour. Further investigations are required to explore the specific mechanisms underlying the retention behaviour differences.

3.4. NP penetration and retention in a flow model

The ability of NPs to penetrate and interact with a thrombus under flow conditions (Fig. 7) was evaluated using a peristaltic pump. The percentage of NPs penetrating and staying in the thrombus was measured as the retention. Under the flow, NPs penetrated the thrombus and remained in the thrombus with a size-dependent tendency. After 4 h of continuous infusion, AUGN10 and AUGN30 showed relatively similar retention percentages within the clot without statistical significance (11.0 ± 0.5% and 9.2 ± 2.0%, respectively, p = 0.09). The larger AUGN100 NPs showed increased retention (44.4 ± 1.1%). Similarly, the retention of AGGN100 in the clot is size-dependent too. AGGN100 was retained more in the clot (42.8 ± 0.3%) than AGGN100 (35.2 ± 0.3%). Overall, these findings indicate that an increase in NP size correlates with enhanced retention within the thrombus. The AGGN100 retention was 9.2% less within the thrombus after the 4 h infusion than the AUGN100 retention. This finding suggests that the silver NPs had less retention effect than the gold NPs. To evaluate the effect of nanoparticle shape, we compared gold nanospheres and AUNRs. The nanorods demonstrated a retention rate of 49.7 ±

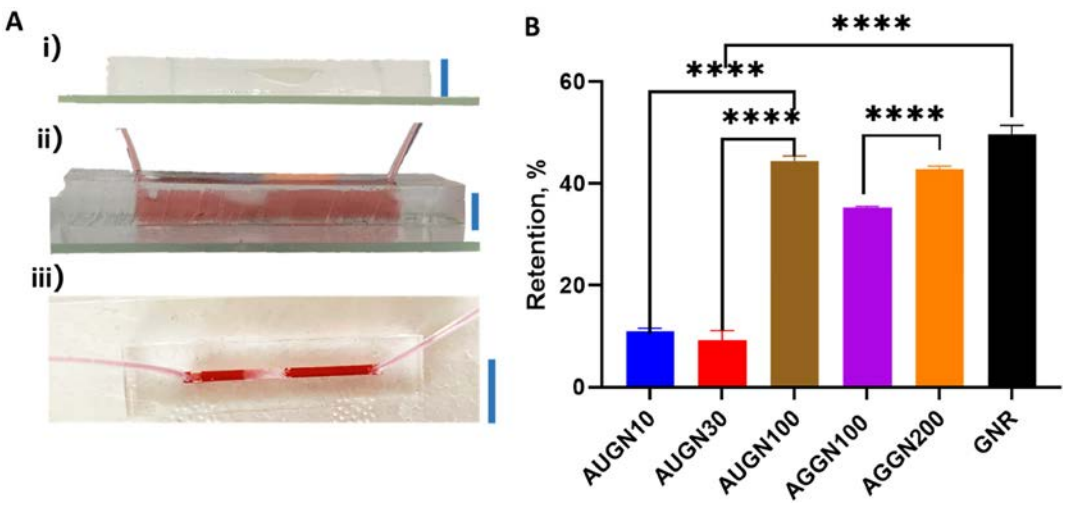

Fig. 7 Nanoparticle penetration through a thrombus under flow conditions. (A) Representative images of the dynamic arterial flow microchannel model (scale bar: 60 mm): (i) side view before nanoparticle solution addition with a thrombus adhered onto the top of the channel, and (ii) side view and (iii) top view of the channel after perfusing AUGN30 (0.25 mg mL^{-1}) solution. (B) Bar chart of the percentages of NPs retained in the thrombus after 4 h perfusion (n = 3–5 per group). AUGN: negatively charged gold nanospheres with a PEG coating, AUBB: positively charged gold nanospheres with a BPEI coating, AGGN: negatively charged silver nanospheres with a PEG coating, and AUNR: negatively charged gold nanorods. *, **, ***, and ****: p < 0.05, 0.01, 0.001 and 0.0001, respectively.

1.8% after four hours. The retention of negatively charged rod shaped NPs was greater in the thrombus than the spherical NPs.

Due to technical limitations, it is important to note that the influence of surface charge on nanoparticle behaviour was not explored in this model. AUBB30 exhibited strong adhesion to tubing and coverslip glass, preventing an accurate assessment of their penetration and retention properties. Therefore, AUBB30 was not tested in a flow model. Future studies should address this limitation to gain a more comprehensive understanding of the role of surface charge in nanoparticle–thrombus retention under flow conditions.

The findings from all models employed in this study were consistent and suggest that NP physiochemical characteristics including size, shape, charge and material all affect the NP penetration and retention in the thrombus. Optimising these parameters is crucial for achieving optimal targeting and drug delivery to the thrombus.

4. Conclusion and future perspectives

Thrombus-induced blockage of blood flow through the vessels in the human body remains the most common killer worldwide. While current treatment options provide a solution with room for improvement, nanoparticle research became more promising with their properties to protect the cargo and capability for targeting. The retention effect is a key concept in understanding the behaviour of nanoparticles within a blood clot. It refers to the extent to which nanoparticles are retained in the thrombus and their ability to diffuse or penetrate through the clot. The current study did not focus on assessing variations in platelet or fibrin density, which may influence the penetration and diffusion of particles within the clot.[36,37] Maintaining consistent thrombus formation conditions, the current study utilised various models to evaluate the penetration and retention capabilities of gold nanoparticles with positive and negative charges, ranging in size from 10 nm to 100 nm, in both spherical and rod shapes, as well as negatively charged silver nanoparticles of 100 nm and 200 nm. The results demonstrate that silver nanoparticles penetrate clots more effectively than their gold counterparts of the same size, and gold nanoparticles tend to remain more within the thrombus. Although their mechanism is currently unclear, this may be due to the ability of Ag nanoparticles to release Ag^+ ions, which could affect the thrombus matrix and facilitate penetration. Further studies are needed to investigate this mechanism. Nanoparticle size significantly influences both penetration and retention. Among particles with similar diameters, rod-shaped nanoparticles exhibited greater retention than spherical ones. Additionally, positively charged nanoparticles showed a higher tendency to be retained in the clot. These findings were consistently observed across the various *in vitro* models used in this study.

Current studies primarily focus on the specific functions of small gold nanospheres with targeted ligands for thrombolysis. However, there has been no comprehensive investigation into the correlation between the physicochemical properties of nanoparticles and their ability to penetrate and be retained in clots. To the best of our knowledge, this is the first study to address this gap by evaluating a range of gold and silver nanoparticles.

Concentration effects (high *vs.* low NP doses) were evaluated using both two-photon microscopy and the thrombus tip model. We found that the overall trends were not significantly affected by concentration. Therefore, in subsequent models we selected a single NP concentration. The cytotoxicity and haemolysis of the NPs were not assessed here as the study's primary aim was to investigate how NP characteristics (size, shape, charge and material) influence clot penetration and retention. Nevertheless, evaluating cytotoxicity and haemolysis across different NP concentrations is essential for future translational studies and should be undertaken for any nanomaterials selected to proceed with thrombolytic therapy.

Future studies could also explore replacing gold and silver with alternative materials for NPs. Additionally, various NP shapes—such as nanocubes, nanostars, and nano-tetrahedra—can be assessed using the models established in this study. Building on these findings, further research may contribute to the development of optimised drug delivery platforms for thrombolysis, ultimately benefiting a broader patient population. The challenges observed with BPEI-coated gold nanospheres (AUBB30) under flow conditions underscore the importance of carefully considering surface chemistry when designing NPs for thrombus targeting. Future work should also investigate alternative positively charged NPs to reduce non-specific interactions and allow accurate assessment of surface charge effects, enabling direct comparisons with negatively charged particles in *in vitro* flow models. Moreover, the development of minimally invasive, advanced imaging techniques to evaluate nanoparticle efficacy in *in vivo* thrombosis models—with real-time distribution tracking—could significantly enhance the understanding of treatment strategies and support their translation into clinical applications.

Conflicts of interest

There are no conflicts to declare.

Data availability

The data supporting this article have been included in the main manuscript and as part of the supplementary information (SI).

Acknowledgements

This study is funded by the National Health and Medical Research Council (HTT: APP1182347 and APP2002827). XC

and HC are supported by PhD scholarships from Griffith University. SSM is supported by a Griffith University fellowship. HTT is supported by a Heart Foundation Future Leader Fellowship (102761) and an Australian Research Council Future Fellowship (FT240100280). We would like to thank the Queensland node of the Australian National Fabrication Facility for access to nano- and microfabrication facilities. Two-photon microscopy was performed at the Institute for Molecular Bioscience Microscopy Facility, which was established with the support of the Australian Cancer Research Foundation (ACRF) and incorporates the Dynamic Imaging, Cancer Biology Imaging and Cancer Ultrastructure and Function Facilities.

References

1 P. Severino, A. D'Amato, M. Pucci, F. Infusino, F. Adamo, L. I. Birtolo, *et al.*, Ischemic Heart Disease Pathophysiology Paradigms Overview: From Plaque Activation to Microvascular Dysfunction, *Int. J. Mol. Sci.*, 2020, **21**(21), 8118.

2 H. Ma, Z. Jiang, J. Xu, J. Liu and Z. N. Guo, Targeted nanodelivery strategies for facilitating thrombolysis treatment in ischemic stroke, *Drug Delivery*, 2021, **28**(1), 357–371.

3 M. Colucci, J. A. Paramo and D. Collen, Inhibition of one-chain and two-chain forms of human tissue-type plasminogen activator by the fast-acting inhibitor of plasminogen activator in vitro and in vivo, *J. Lab. Clin. Med.*, 1986, **108**(1), 53–59.

4 W. J. Powers, A. A. Rabinstein, T. Ackerson, O. M. Adeoye, N. C. Bambakidis, K. Becker, *et al.*, Guidelines for the Early Management of Patients With Acute Ischemic Stroke: A Guideline for Healthcare Professionals From the American Heart Association/American Stroke Association, *Stroke*, 2018, **49**(3), e46–e110.

5 X. Chen, Y. Wu, V. T. Dau, N. T. Nguyen and H. T. Ta, Polymeric nanomaterial strategies to encapsulate and deliver biological drugs: points to consider between methods, *Biomater. Sci.*, 2023, **11**(6), 1923–1947.

6 N. A. Fithri, Y. Wu, G. Cowin, F. Akther, H. D. N. Tran, B. Tse, *et al.*, Gold-iron oxide nanoparticle: A unique multimodal theranostic approach for thrombosis, *Appl. Mater. Today*, 2023, **31**, 101750.

7 H. Ta, S. Prabhu, E. Leitner, K. Putnam, F. Jia, N. Bassler, *et al.*, A Novel Biotechnological Approach for Targeted Regenerative Cell Therapy and Molecular Imaging of Atherothrombosis, *Heart, Lung Circ.*, 2010, **19**, S10.

8 H. T. Ta, N. Arndt, Y. Wu, H. J. Lim, S. Landeen, R. Zhang, *et al.*, Activatable magnetic resonance nanosensor as a potential imaging agent for detecting and discriminating thrombosis, *Nanoscale*, 2018, **10**(31), 15103–15115.

9 K. X. Vazquez-Prada, S. S. Moonshi, Y. Wu, F. Akther, B. W. C. Tse, K. A. Sokolowski, *et al.*, A Spiky Silver-Iron Oxide Nanoparticle for Highly Efficient Targeted Photothermal Therapy and Multimodal Imaging of Thrombosis, *Small*, 2023, **19**(11), 2205744.

10 K. X. Vazquez-Prada, S. S. Moonshi, Y. Wu, K. Peter, X. Wang, Z. P. Xu, *et al.*, Branched silver–iron oxide nanoparticles enabling highly effective targeted and localised drug-free thrombolysis, *Biomater. Sci.*, 2025, **13**, 1683–1696.

11 K. X. Vazquez-Prada, S. S. Moonshi, Z. P. Xu and H. T. Ta, Photothermal nanomaterials for theranostics of atherosclerosis and thrombosis, *Appl. Mater. Today*, 2023, **35**, 101967.

12 R. Au, Y. Wu, H. Tran, K. Vazquez-Prada, Y. Liu, H. Adelnia, *et al.*, Silver/iron oxide nano-popcorns for imaging and therapy, *ACS Appl. Nano Mater*, 2021, **4**(10), 10136–10147.

13 K. X. Vazquez-Prada, J. Lam, D. Kamato, Z. P. Xu, P. J. Little and H. T. Ta, Targeted molecular imaging of cardiovascular diseases by iron oxide nanoparticles, *Arterioscler., Thromb., Vasc. Biol.*, 2021, **41**(2), 601–613.

14 N. Arndt, H. D. Tran, R. Zhang, Z. P. Xu and H. T. Ta, Different approaches to develop nanosensors for diagnosis of diseases, *Adv. Sci.*, 2020, **7**(24), 2001476.

15 N. N. M. Yusof, A. McCann, P. J. Little and H. T. Ta, Non-invasive imaging techniques for the differentiation of acute and chronic thrombosis, *Thromb. Res.*, 2019, **177**, 161–171.

16 H. T. Ta, Z. Li, C. E. Hagemeyer, G. Cowin, S. Zhang, J. Palasubramaniam, *et al.*, Molecular imaging of activated platelets via antibody-targeted ultra-small iron oxide nanoparticles displaying unique dual MRI contrast, *Biomaterials*, 2017, **134**, 31–42.

17 H. T. Ta, S. Prabhu, E. Leitner, F. Jia, D. von Elverfeldt, K. E. Jackson, *et al.*, Enzymatic single-chain antibody tagging: a universal approach to targeted molecular imaging and cell homing in cardiovascular disease, *Circ. Res.*, 2011, **109**(4), 365–373.

18 A. Refaat, B. del Rosal, J. Palasubramaniam, G. Pietersz, X. Wang, S. E. Moulton, *et al.*, Near-infrared light-responsive liposomes for protein delivery: Towards bleeding-free photothermally-assisted thrombolysis, *J. Controlled Release*, 2021, **337**, 212–223.

19 A. Refaat, B. del Rosal, V. Bongcaron, A. P. G. Walsh, G. Pietersz, K. Peter, *et al.*, Activated Platelet-Targeted IR780 Immunoliposomes for Photothermal Thrombolysis, *Adv. Funct. Mater.*, 2023, **33**(4), 2209019.

20 G. Alkarithi, C. Duval, Y. Shi, F. L. Macrae and R. A. S. Ariëns, Thrombus Structural Composition in Cardiovascular Disease, *Arterioscler., Thromb., Vasc. Biol.*, 2021, **41**(9), 2370–2383.

21 M. A. Mackey, M. R. K. Ali, L. A. Austin, R. D. Near and M. A. El-Sayed, The Most Effective Gold Nanorod Size for Plasmonic Photothermal Therapy: Theory and In Vitro Experiments, *J. Phys. Chem. B*, 2014, **118**(5), 1319–1326.

22 J. Viereck, F. L. Ruberg, Y. Qiao, A. S. Perez, K. Detwiller, M. Johnstone, *et al.*, MRI of atherothrombosis associated with plaque rupture, *Arterioscler., Thromb., Vasc. Biol.*, 2005, **25**(1), 240–245.

23 B. Zhang and X. Jiang, Magnetic Nanoparticles Mediated Thrombolysis-A Review, *IEEE Open J. Nanotechnol.*, 2023, **4**, 109–132.

24 D. Qin, Y. Xia and G. M. Whitesides, Soft lithography for micro- and nanoscale patterning, *Nat. Protoc.*, 2010, **5**(3), 491–502.
25 H. Cha, H. A. Amiri, S. Moshafi, A. Karimi, A. Nikkhah, X. Chen, *et al.*, Effects of obstacles on inertial focusing and separation in sinusoidal channels: An experimental and numerical study, *Chem. Eng. Sci.*, 2023, **276**, 118826.
26 N. Mina, V. S. Guido, A. F. Lima, M. L. V. Oliva and A. A. Sousa, Ultrasmall Nanoparticles Bind to Fibrinogen and Impair Normal Clot Formation, *Part. Part. Syst. Charact.*, 2024, **41**(4), 2300107.
27 F. Helmchen and W. Denk, Deep tissue two-photon microscopy, *Nat. Methods*, 2005, **2**(12), 932–940.
28 C. S. Lim and B. R. Cho, Two-photon probes for biomedical applications, *BMB Rep.*, 2013, **46**(4), 188–194.
29 M. Ye, X. Yu, Y. Yuan, M. He, J. Zhuang, S. Xiong, *et al.*, Design a dual-response two-photon fluorescent probe for simultaneous imaging of mitochondrial viscosity and peroxynitrite in a thrombosis model, *Anal. Chim. Acta*, 2024, **1287**, 342088.
30 M. M. Kamocka, J. Mu, X. Liu, N. Chen, A. Zollman, B. Sturonas-Brown, *et al.*, Two-photon intravital imaging of thrombus development, *J. Biomed. Opt.*, 2010, **15**(1), 016020.
31 M. Okano, T. Hara, M. Nishimori, Y. Irino, S. Satomi-Kobayashi, M. Shinohara, *et al.*, In Vivo Imaging of Venous Thrombus and Pulmonary Embolism Using Novel Murine Venous Thromboembolism Model, *JACC*, 2020, **5**(4), 344–356.
32 N. Mackman, Triggers, targets and treatments for thrombosis, *Nature*, 2008, **451**(7181), 914–918.
33 H. Wang, K. W. Bang, V. S. Blanchette, A. T. Nurden and M. L. Rand, Phosphatidylserine exposure, microparticle formation and mitochondrial depolarisation in Glanzmann thrombasthenia platelets, *Thromb. Haemostasis*, 2014, **111**(6), 1184–1186.
34 Q. Abbas, B. Yousaf, Amina, M. U. Ali, M. A. M. Munir, A. El-Naggar, *et al.*, Transformation pathways and fate of engineered nanoparticles (ENPs) in distinct interactive environmental compartments: A review, *Environ. Int.*, 2020, **138**, 105646.
35 R. Ungricht, M. Klann, P. Horvath and U. Kutay, Diffusion and retention are major determinants of protein targeting to the inner nuclear membrane, *J. Cell Biol.*, 2015, **209**(5), 687–703.
36 J. J. Hathcock and Y. Nemerson, Platelet deposition inhibits tissue factor activity: in vitro clots are impermeable to factor Xa, *Blood*, 2004, **104**(1), 123–127.
37 T. J. Stalker, E. A. Traxler, J. Wu, K. M. Wannemacher, S. L. Cermignano, R. Voronov, *et al.*, Hierarchical organization in the hemostatic response and its relationship to the platelet-signaling network, *Blood*, 2013, **121**(10), 1875–1885.